to the flat bottom dielectric slabs, and tested them with a $4 \times 2$ array antenna. This modification makes the shape of slabs similar to the one shown in Figure 8. Figure 9 shows the H-plane radiation patterns of three cases. With the addition of small notches, the antenna beam can now be scanned up to $+40°$.

## 5. CONCLUSIONS

A novel design of a steerable array antenna has been demonstrated. The phase shifter is based on a movable dielectric slab placed close to a CPW with air gaps. The impedance mismatch can be avoided by choosing the slab dielectric constant and length for the two extreme positions, namely at $d = 0$ and $d$ 2 mm. It may be possible to further reduce $S_{11}$ by optimizing the impedance mismatching position at $d > 0$ instead of $d = 0$. We also show that the use of preset delay lines can reduce the number of phase shifters. Although the test antenna is designed for 5.8 GHz, the technique can be applied at a much higher frequency. One possible application is for the 77 GHz automobile collision avoidance radar [6].


## ACKNOWLEDGMENTS

This project was supported by National Science Foundation ECS-0424414. The authors thank J. Kajiya and J. Ritcey for useful discussions and suggestions.


## REFERENCES


1. Y. Kuga, J. Cha, J.A. Ritcey, and T. Kajiya, Mechanically steerable antennas using dielectric phase shifters, IEEE AP-S International Symposium, Monterey, CA, 2004, pp. 161–164.
2. J. Baker-Jarvis and E.J. Vanzura, Improved technique for determining complex, permittivity with the transmission/reflection method, IEEE Trans Microwave Theory Tech 38 (1990), 1096–1101.
3. J. Cha, Y. Kuga, and T. Kajiya, Mechanically steerable antennas with controllable, microwave phase shifters at 20 GHz, IEEE AP-S International Symposium, Washington D.C, 2005, pp. 691–694.
4. C.F. Wang, F. Ling, and J.M. Jin, A fast full-wave analysis of scattering and radiation from large finite arrays of microstrip antennas, IEEE Trans Antennas Propagat AP-46 (1998), 1467–1474.
5. K.L. Wu, M. Spenuk, J. Litva, and D.G. Fang, Theoretical and experimental study of feed network effects on the radiation pattern of series-fed microstrip antenna arrays, IEE Proceedings-H 138 (1991), No. 3.
6. J. Cha and Y. Kuga, A mechanically steerable array antenna using controllable dielectric phase shifters for 77 GHz automotive radar systems, IEEE AP-S International Symposium, Albuquerque, NM, 2006.




# GROWTH AND STUDIES OF OPTICAL PROPERTIES OF DOUBLE-DOPED In: Fe:$LiTaO_3$ CRYSTAL


**Decai Ma,[1] Biao Wang,[1,2,3] Shuangquan Fang,[1] Tao Zhang,[1] Rui Wang,[1] and Yuan Wei[1]**

[1] School of Astronautics
Harbin Institute of Technology
Harbin 150001, China
[2] State Key Laboratory of Optoelectronic Materials and Technologies
Institute of Optoelectronic and Functional Composite Materials
Sun Yat-Sen University
Guangzhou 510275, China
[3] School of Physics Science and Engineering
Sun Yat-Sen University
Guangzhou 510275, China



*Received 16 April 2006*



**ABSTRACT:** *In:Fe:$LiTaO_3$ crystals were grown in an air atmosphere using the Czochralski method. The photorefractive properties were measured by the two-wave coupling experiments, and light-induced scattering was used to characterize the optical damage. It was found that the photorefractive response speed of In:Fe:$LiTaO_3$ was about four times faster than that of Fe:$LiTaO_3$, and the resistance ability to optical damage was drastically improved. The increase in damage resistance and faster response speed could be attributed to the $Fe^{3+}$ losing their electron acceptor properties and, therefore, an increase in photoconductivity.* © 2006 Wiley Periodicals, Inc. Microwave Opt Technol Lett 48: 2227–2230, 2006; Published online in Wiley InterScience (www.interscience.wiley.com). DOI 10.1002/mop.21919



**Key words:** *In:Fe:$LiTaO_3$ crystal; exponential gain coefficient; diffraction efficiency; response speed; photodamage resistance*


## 1. INTRODUCTION

Doped lithium tantalum ($LiTaO_3$, LT) crystals exhibit excellent photorefractive properties, and this attractive feature makes them important for applications in piezoelectric, electro-optic, surface acoustic wave, waveguide, and nonlinear optical devices [1– 5]. Doping with transition metal or rare earth ions into crystals can affect efficiency, sensitivity, speed, and spectral response of photorefractive effect. A great amount of studies on $LiTaO_3$ included crystals containing various dopants, such as Fe, Ce [6], Zn [7], Cr [8], Tm [9], Ho [10], and so on. Fe:$LiTaO_3$ crystal has been selected as one of holographic storage media for industrial use. In Fe:$LiTaO_3$ crystal, $Fe^{2+}$ ions acted as electron donors, and $Fe^{3+}$ ions act as electron traps. Electrons are excited from $Fe^{2+}$ to the conduct band, and then are redistributed because of diffusion, drift, and bulk photovoltaic effect. Finally, $Fe^{3+}$ will capture the electrons and a space charge field builds up. The refractive index can be modulated by electro-optic effect. Fe:$LiTaO_3$ crystal has the promising application in the volume holographic storage, but there are some disadvantages, e.g. long response time and low photodamage resistance ability. For improving photodamage resistance ability of Fe:$LiTaO_3$ crystal, in this work, $In_2O_3$ was doped into Fe:$LiTaO_3$ crystal. In:Fe:$LiTaO_3$ crystals grown by Czochralski (CZ) method show excellent photodamage resistance ability. In addition, the response time of the In:Fe:$LiTaO_3$ crystal decreased to a acceptable degree in comparison with Fe:$LiTaO_3$ crystal.

## 2. CRYSTAL GROWTH AND SPECIMEN PREPARATION

All crystals including Fe:$LiTaO_3$, In:Fe:$LiTaO_3$, Fe:$LiNbO_3$, and In:Fe:$LiNbO_3$, are grown from congruent melts by the conventional CZ method, using an intermediate frequency(IF) furnace. The starting materials used to grow the crystals were $Fe_2O_3$, $In_2O_3$,

**TABLE 1 Summary of Doping Levels and Composition for the Crystals**

| Crystal | Fe:$LiTaO_3$ | In:Fe:$LiTaO_3$ | Fe:$LiNbO_3$ | In:Fe:$LiNbO_3$ |
|---|---|---|---|---|
| [$In_2O_3$] (mol %) | 0 | 3 | 0 | 3 |
| [$Fe_2O_3$] (wt %) | 0.03 | 0.03 | 0.03 | 0.03 |
| [Li]/[Ta] (mol ratio) | 0.951 | 0.951 | – | – |
| [Li]/[Nb] (mol ratio) | – | – | 0.946 | 0.946 |
| Growth atmosphere | Air | Air | Air | Air |

$Li_2CO_3$, $Nb_2O_5$, and $Ta_2O_5$, which were all of 99.99% purity. Compositions of the raw materials were shown in Table 1.

The crystal was pulled along (001) direction at a rate of 2–4 mm/h and a rotating rate of 10–20 rpm, and the axial temperature gradient of the IF furnace was 30–35°C/cm. After growth, the crystals were cooled down to room temperature at a rate of 50°C/h. The crystals were then polarized in another resistive furnace in which the temperature gradient was almost close to zero, using an applied DC electric density of 10–15 mA/cm$^2$ for 15 min at 700°C. All as-grown crystals appeared to be transparent, crack-free, and inclusion-free. Lastly, from the middle of the crystals, they were y-cut into slices with the size of $5 \times 2 \times 5$ mm$^3$ ($a \times b \times c$). The (010) faces were ground using SiC powder and then polished to optical grade using a 0.25 $\mu$m diamond solution, for experimental characterization.

## 3. MEASURE OF PHOTOREFRACTIVE PROPERTIES

### *3.1. Exponential Gain Coefficient*

The exponential gain coefficient is one of the important indicators to evaluate the photorefractive sensitivity of crystals, which indicates the ability to transit energy from the pump light with high power to signal light. Two-beam coupling experiments were used to measure the exponential gain coefficient. Figure 1 shows the typical experimental setup of two-beam coupling. Both a weak probe wave (signal beam $I_S$) and a pump wave (reference beam $I_P$) originated from $Ar^+$ laser (wavelength $\lambda = 514.5$ nm) were irradiated on a sample with polarization direction parallel to the $c$-axis of the sample. Then, intensive beam coupling occurred and caused the signal beam intensity enhanced at the expense of the reference beam. The exponential gain coefficient $\Gamma$ can be described by the following equation [11]:

$$\Gamma = \frac{1}{L} \ln\left(\frac{I'_{ST} I_{PT}}{I_{ST} I'_{PT}}\right), \tag{1}$$

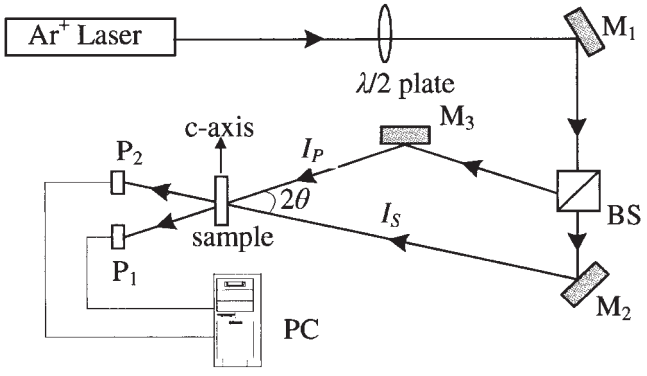


**Figure 1** Experimental setup of two-wave mixing experiment. Experimental setup of two-wave mixing experiment. $M_1$, $M_2$, and $M_3$: mirrors; BS: beam splitter; D: detector; $P_1$, $P_2$: photocell; PC: computer; $I_p$, $I_s$: pump light and signal light

where $L$ is the interaction length of the two beams in crystal (taken as the thickness of the sample), $I'_{ST}$ ($I_{ST}$) is the transmitted signal beam intensity with (without) coupling, and $I'_{PT}$ ($I_{PT}$) is the transmitted pump beam intensity with (without) coupling. When the intensity of pump beam is much larger than that of signal beam, $I_{PT} \gg I_{ST}$, the two-beam coupling gain coefficient $\Gamma$ becomes independent of the pump beam intensity (i.e. $I'_{PT} \approx I_{PT}$). Thus Eq. (1). can be simplified as

$$\Gamma = \frac{1}{L} \ln \frac{I'_S}{I_S}. \tag{2}$$

In the experiment, the diameters of the pump and the signal beam were both adjusted to 1 mm. The ratio of light intensity was $m = 1820$. After the signal beam coupled, the intensity of the signal beam and the angle between the pump and the signal beam were recorded. The exponential gain coefficient, $\Gamma$, related to the angle of the two beams can be described by the following equation

$$\Gamma = \left[\frac{A \sin\theta}{1 + B^{-2} \sin^2\theta}\right]\left(\frac{\cos 2\theta_1}{\cos\theta_1}\right), \tag{3}$$

where the $\theta$ is the external half angle, $\theta_1$ is the internal half angle between the two incident laser beams, $A$ is determined by the slope of the plot of $\Gamma$ vs. $2\theta$ near $\theta = 0$, and the parameter $B$ is determined by $\theta_{peak}$.

### *3.2. Diffraction Efficiency and Response Time*

Diffraction efficiency and response time were also measured by the two-wave coupling experiment. The experimental light path scheme is shown in Figure 1. $Ar^+$ laser with a wavelength of 514.5 nm was used, in which the intensity was 1.34 W/cm$^{-2}$. The diffraction efficiency $\eta$ was described as the ratio between diffractive and transmitting intensities,

$$\eta = \frac{I'_{SD}}{(I'_{SD} + I_{ST})} \times 100\%, \tag{4}$$

where $I'_{SD}$ is the diffractive intensity of $I_S$ after the grating was built, and $I_{ST}$ is the transmitting intensity of $I_S$ before the grating was built.

The response time is defined as the time interval that is from the time of incident light beginning to shot on the crystal to the time when the diffraction efficiency reaches its maximum. The measured results were shown in Table 2.

**TABLE 2 Optical Properties of the $LiTaO_3$ and $LiNbO_3$ Samples**

| Crystal | Fe:$LiTaO_3$ | In:Fe:$LiTaO_3$ | Fe:$LiNbO_3$ | In:Fe:$LiNbO_3$ |
|---|---|---|---|---|
| $\tau$(s) | 71 | 18 | 290 | 47 |
| $\eta$ (%) | 57 | 41 | 64 | 46 |

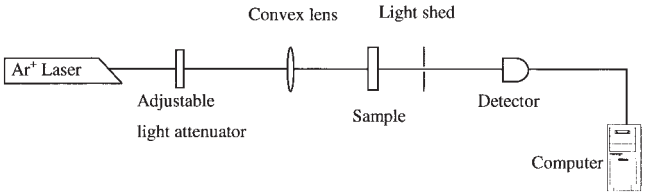


**Figure 2** Experimental setup of the light-scattering resistance ability

## 4. OPTICAL DAMAGE RESISTANCE OF In:Fe:$LiTaO_3$

When $LiTaO_3$ crystals are used as volume holographic storage media, higher light-induced scattering resistance ability can improve the quality of the storage information, suppress the generation of noise, and reduce the bit error rate. To obtain the ability of the In:Fe:$LiTaO_3$ to resist photorefraction, the light-induced scattering change of a transmitted laser beam through the 2-mm-thick plates of these crystals was measured. The experimental setup was shown in Figure 2. An $Ar^+$ laser beam (wavelength, 514.5 nm), whose intensity can be controlled by the adjustable light attenuator, irradiated to the crystals was placed on the focal plane of the lens. The optical damage threshold value $R$ of the crystal was defined as the ratio of the light scattered intensity $I'$ to the incident light intensity $I$, $R = I'/I$, in the crystals as a function of $I$.

## 5. RESULTS AND DISCUSSION

The experimental results of the exponential gain coefficient are shown in Figure 3. The figure shows that In:Fe:$LiTaO_3$ crystal had a maximal exponential gain coefficient ($\Gamma_{max}$) of 19.2/$cm^{-1}$ at an angle of about 20°. The main reason for the higher exponential gain coefficient in a large angle range may be the intensive light crawling effect that existed in the thinner In:Fe:$LiTaO_3$ crystal, similar to that in $LiNbO_3$ [12].

Figure 4 shows the experimental results of the diffractive efficiency $\eta$ relating to $2\theta$. The experimental results indicate that the diffractive efficiency of the In:Fe:$LiTaO_3$ crystal reaches a maximum of 41% at about an angle of 21°. The response speed of the In:Fe:$LiTaO_3$ crystal from Table 2 approached four times higher than that of Fe:$LiTaO_3$ and also higher than that of In:Fe:$LiNbO_3$ crystal.

Figure 5 gives the curves of the ratio $R$ relating to the incident light intensity $I$. From Figure 5, it can be observed that the photodamage resistances of the In:Fe:$LiTaO_3$ crystal magnitude were higher than that of the Fe:$LiTaO_3$ and was also higher than that of the In:Fe:$LiNbO_3$ crystal.

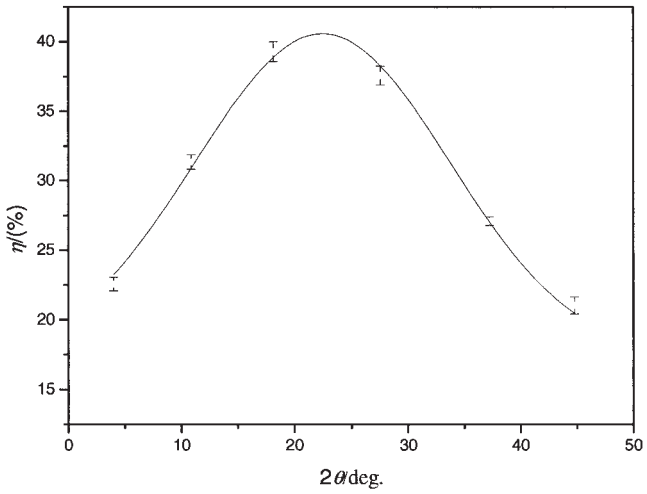


**Figure 4** The experimental results between diffractive efficiency $\eta$ and $2\theta$

Lots of Li-deficient ([Li]/[Ta] < 1) present in the congruent $LiTaO_3$ crystal. Therefore, there are a lot of intrinsic defects in the $LiTaO_3$ crystal, such as anti-site tantalum ($Ta_{Li}^{4+}$) and lithium vacancy ($V_{Li}^{-}$) defects. In Fe-doped $LiTaO_3$, a reduced capture section of $Fe^{3+}$ is responsible for the observed increase in photoconductivity, because $Fe^{3+}$ ions are the most probable electron acceptors. Other doping ions incorporated into the host lattice will change the substitution site of electron acceptor $Fe^{3+}$. There should be fewer intrinsic defects in congruent $LiTaO_3$ than that in congruent $LiNbO_3$ for [Li]/[Ta] > [Li]/[Nb]. Threshold concentration of $In_2O_3$ is about 3 mol % in the congruent $LiNbO_3$ crystal, and so the $In_2O_3$ concentration has exceeded its threshold in congruent $LiTaO_3$ doping with 3 mol % $In_2O_3$. When doping $Fe^{3+}$ in the $LiTaO_3$ crystal, $Fe^{3+}$ will replace $Ta_{Li}^{4+}$ and $Ta^{5+}$ simultaneously. This will cause photoconductivity is governed by the electron acceptor $Fe^{3+}$, since the content of $Ta_{Li}^{4+}$ decrease. After $In_2O_3$ doped into the Fe:$LiTaO_3$, $In^{3+}$ takes the priority of replacing $Ta_{Li}^{4+}$ and $Fe^{3+}$ replaces $Ta_{Li}^{4+}$ and $Ta^{5+}$ simultaneously. When

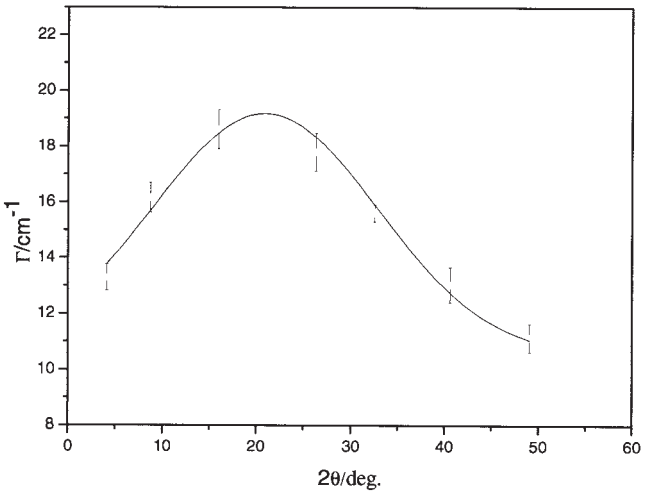


**Figure 3** The experimental results between exponential gain coefficient $\Gamma$ and $2\theta$

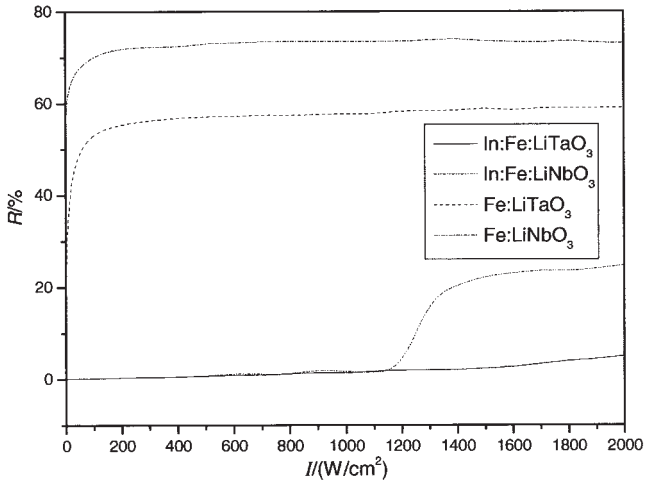


**Figure 5** Dependence of the ratio $R$ of the light-scattered intensity to the incident light intensity vs. the incident light intensity

$In_2O_3$ doping exceeds its threshold in Fe:$LiTaO_3$ crystal, all $Ta_{Li}^{4+}$ were replaced completely, and $Fe^{3+}$ ions will be pushed to $Ta^{5+}$ site and lost their electron acceptor properties, since $Fe_{Nb}^{2-}$ defects were electronegative. This drastically increased in photoconductivity. Therefore, the resistance ability to optical damage of the In (3 mol %):Fe (0.03%):$LiTaO_3$ crystal was much higher than that of the other crystals (Fig. 5). The response speed becomes also fast because of the increased photoconductivity by doping $In^{3+}$ in the Fe: $LiTaO_3$ crystal. Because increased photoconductivity indicated that motion of photoinduced charge carriers would become fast, which made the space charge field form faster, photorefractive response speed increased.

## 6. CONCLUSIONS

In conclusion, we grew crack-free and inclusion-free In, Fe co-doped $LiTaO_3$, and $LiNbO_3$ single crystals by CZ method, and studied its optical properties. The measured results showed that the photorefractive response speed can be greatly improved by doping $In_2O_3$ in Fe:$LiTaO_3$, and the resistance ability to photodamage of In:Fe:$LiTaO_3$ crystal was magnitude higher than that of Fe:$LiTaO_3$ crystal. Our analysis indicated that the increased photoconductivity improved both fast photorefractive response and high photodamage resistance in the In:Fe:$LiTaO_3$ crystal.


## ACKNOWLEDGMENTS

This work was supported by the National Natural Science Foundation of China (50232030, 10172030), The National Science Foundation of Heilongjiang Province, The Ministry of Science and Technology of China through the High-Tech Program (2001AA31304), and the National Committee of Defense, Science and Technology.


## REFERENCES


1. Y. Wang and Y.J. Jiang, Crystal orientation dependence of piezoelectric properties in $LiNbO_3$ and $LiTaO_3$, Opt Mater 23 (2003), 403–408.
2. I. Reinhard, M. Gabrysch, B.F.V. Weikersthal, K. Jungmann, and G.Z. Putlitz, Measurement and compensation of frequency chirping in pulsed dye laser amplifiers, Appl Phys B 63 (1996), 467–472.
3. A. Holm, Q. Stürzer, Y. Xu, and R. Weigel, Investigation of surface acoustic waves on $LiNbO_3$, quartz, and $LiTaO_3$ by laser probing, Microelectron Eng 31 (1996), 123–127.
4. M.K. Kuneva, S.H. Tonchev, and P.A. Atanasov, Infrared spectra of proton-exchanged waveguides in $LiNbO_3$ and $LiTaO_3$, Mater Sci Eng B 118 (2005), 301–305.
5. Y.N. Korkishko, V.A. Fedorov, S.M. Kostritskii, A.N. Alkaev, E.I. Maslennikov, E.M. Paderin, D.V. Apraksin, and F. Laurell, Proton exchanged $LiNbO_3$ and $LiTaO_3$ optical waveguides and integrated optic devices, Microelectron Eng 69 (2003), 228–236.
6. B.K. Kim, G.Y. Kang, J.K. Yoon, and J.H. Ro, The photorefractive effects of Fe and Fe plus Ce doped $LiTaO_3$ single crystal, J Phys Chem Solid 61 (2000), 637–646.
7. S.F. Fang, B. Wang, T. Zhang, F.R. Ling, and R. Wang, Growth and photo refractive properities of Zn, Fe double-doped $LiTaO_3$ crystal, Opt Mater 28 (2006), 207–211.
8. I. Sokolska and S. Kuck, Optical characterization of $Cr^{3+}$ doped $LiTaO_3$ crystals relevant for laser application, Spectrochim Acta A 54 (1998), 1695–1700.
9. I. Sokólska, W. Ryba-Romanowski, S. Golab, M. Baba, M. Swirkowicz, and T. Lukasiewicz, Spectroscopy of $LiTaO_3$:$Tm^{3+}$ crystals, J Phys Chem Solid 61 (2000), 1573–1581.
10. I. Sokolska, Infrared to visible conversion of radiation in some $Ho^{3+}$-doped oxide and fluoride crystals, J Alloys Compd 341 (2002), 288–293.
11. C.H. Yang, Y.Q. Zhao, R. Wang, and M.H. Li, Studies of photorefractive crystals of double-doped Ce,Fe:$LiNbO_3$, Opt Commun 175 (2000), 247–252.
12. J. Zhang, W. Sun, H. Zhao, S. Bian, K. Xu, M. Li, and Y. Xu, Enhancement of the exponential gain coefficient as a result of the light-fanning effect in thin doped $LiNbO_3$ crystals, Opt Lett 18 (1993), 1391–1393.




# DESIGN AND FABRICATION OF INTEGRATED FILM BULK ACOUSTIC RESONATOR AND FILTER ON SILICON NITRIDE MEMBRANE


**Jae Yoeng Park,[1] Hee Chul Lee,[2] and Seong Jong Cheon[1]**

[1] Department of Electronic Engineering
Kwangwoon University
447–1
Wolgye-Dong
Nowon-Gu
Seoul 139–701
Republic of Korea

[2] Materials and Devices Laboratory
LG Electronics Institute of Technology
Woomyeon-Dong
Seocho-Gu
Seoul 137–724
Republic of Korea


*Received 30 March 2006*


**ABSTRACT:** *In this paper, fully integrated film bulk acoustic resonators (FBARs) and filter have been designed, fabricated, and characterized by using silicon bulk micromachining technology. The fabricated resonator is comprised of aluminum nitride (AlN) piezoelectric material sandwiched by two molybdenum (Mo) electrodes on top of silicon nitride thin membrane. The developed AlN piezoelectric film has 1.9° of FWHM (full width half maximum) of rocking curve and approximately 70 Mpa in tensile stress on top of the Mo electrode. The fabricated FBAR has a quality factor of 1530 in size of 200 × 200 $\mu m^2$, insertion loss of −0.45 dB, and return loss of −28 dB, respectively. The fabricated FBAR ladder type filter is comprised of 7 resonators with 3 resonators in series and 4 resonators in parallel. It has insertion loss of −3.2 dB and ripple of 0.4 dB in pass band, absolute attenuation of 40 and 50 dB at 1.6–1.875 GHz and 2.110–2.170 GHz, respectively. The size of the fabricated FBAR filter is 1.2 mm × 1.4 mm before packaging and 3 mm × 3 mm after packaging, respectively.* © 2006 Wiley Periodicals, Inc. Microwave Opt Technol Lett 48: 2230–2233, 2006; Published online in Wiley InterScience (www.interscience.wiley.com). DOI 10.1002/mop.21905


**Key words:** *piezoelectricity; FBAR; resonators; band pass filters; acoustic waves; Micromachining; AIN; molybdenum*

## 1. INTRODUCTION

Recently, there are great demands for RF band pass filters with smaller size/volume, lighter weight, and higher performance for advanced mobile communication handset systems. However, the current filter technology using lumped LC elements, ceramic resonators [1], and surface acoustic wave (SAW) resonators [2,3] have difficulties in on-chip integration, power handling capability, and temperature compensation [4]. Thus, the FBARs have been considerably attracted for fabricating the RF filters with small size and volume. The FBARs have much more smaller size than dielectric resonators and lumped LC elements, lower insertion loss (IL) and higher power handling capabilities than SAW devices, and full integration with other CMOS/RF IC circuitry for realizing a single chip radio or a transceiver.